Acta Biomaterialia 72 (2018) 434–446

Contents lists available at ScienceDirect

Acta Biomaterialia

journal homepage: www.elsevier.com/locate/actabiomat

Full length article

Cobalt (II) ions and nanoparticles induce macrophage retention by ROS-mediated down-regulation of RhoA expression

Jing Xu [a], Junyao Yang [b], Agata Nyga [c,d], Mazdak Ehteramyan [e], Ana Moraga [e], Yuanhao Wu [a], Lingfang Zeng [e,*], Martin M. Knight [a,*], Julia C. Shelton [a,*]

[a] Institute of Bioengineering, School of Engineering and Materials Science, Queen Mary University of London, London, UK
[b] Department of Laboratory Medicine, Xinhua Hospital, School of Medicine, Shanghai Jiao Tong University, Shanghai 200092, China
[c] Division of Surgery and Interventional Sciences, University College London, London NW3 2QG, United Kingdom
[d] Institute for Bioengineering of Catalonia, 08028 Barcelona, Spain
[e] Cardiovascular Division, Faculty of Life Science and Medicine, King's College London, London SE5 9NU, United Kingdom

ARTICLE INFO

Article history:
Received 18 November 2017
Received in revised form 15 March 2018
Accepted 30 March 2018
Available online 9 April 2018

Keywords:
Cobalt chromium
Nanoparticles
Wear debris
Macrophage
ROS

ABSTRACT

Histological assessments of synovial tissues from patients with failed CoCr alloy hip prostheses demonstrate extensive infiltration and accumulation of macrophages, often loaded with large quantities of particulate debris. The resulting adverse reaction to metal debris (ARMD) frequently leads to early joint revision. Inflammatory response starts with the recruitment of immune cells and requires the egress of macrophages from the inflamed site for resolution of the reaction. Metal ions (Co^{2+} and Cr^{3+}) have been shown to stimulate the migration of T lymphocytes but their effects on macrophages motility are still poorly understood. To elucidate this, we studied *in vitro* and *in vivo* macrophage migration during exposure to cobalt and chromium ions and nanoparticles. We found that cobalt but not chromium significantly reduces macrophage motility. This involves increase in cell spreading, formation of intracellular podosome-type adhesion structures and enhanced cell adhesion to the extracellular matrix (ECM). The formation of podosomes was also associated with the production and activation of matrix metalloproteinase-9 (MMP9) and enhanced ECM degradation. We showed that these were driven by the down-regulation of RhoA signalling through the generation of reactive oxygen species (ROS). These novel findings reveal the key mechanisms driving the wear/corrosion metallic byproducts-induced inflammatory response at non-toxic concentrations.

Statement of significance

Adverse tissue responses to metal wear and corrosion products from CoCr alloy implants remain a great challenge to surgeons and patients. Macrophages are the key regulators of these adverse responses to the ions and debris generated. We demonstrated that cobalt, rather than chromium, causes macrophage retention by restructuring the cytoskeleton and inhibiting cell migration via ROS production that affects Rho Family GTPase. This distinctive effect of cobalt on macrophage behaviour can help us understand the pathogenesis of ARMD and the cellular response to cobalt based alloys, which provide useful information for future implant design and biocompatibility testing.

1. Introduction

Total hip arthroplasty (THA) restores mobility and improves the quality of life in patients suffering from severe osteoarthritis or femoral fractures. In 2015, 83,886 primary hip replacements were conducted in the UK with 8,367 hip revision procedures performed largely due to the aseptic loosening, pain, implant wear and adverse reaction to metal debris (ARMD) [1]. It is expected that these numbers will keep rising due to the ageing of population and an increasing number of implanted prostheses.

Since the mid-1980 s, over one million metal-on-metal (MoM) hip replacement prostheses, made from a cobalt chromium (CoCr) alloy, have been implanted worldwide [2]. These were used for joint replacements in younger, more active patients [3] due to

* Corresponding authors.
E-mail addresses: lingfang.zeng@kcl.ac.uk (L. Zeng), m.m.knight@qmul.ac.uk (M.M. Knight), j.shelton@qmul.ac.uk (J.C. Shelton).

https://doi.org/10.1016/j.actbio.2018.03.054
1742-7061/

the adverse response to polyethylene particles from the first-generation metal-on-polyethylene (MoP) bearings or from the fracture risk of a ceramic head. However, concerns for these implants became increasingly prominent due to reports of ARMD [4,5]. The metal wear debris and released ions (Co^{2+} and Cr^{3+}), which are widely generated in MoM bearings of hip implants, are now also found in patients with MoP bearings due to the mechanically assisted crevice corrosion of modular taper junctions, including head–neck and neck-stem taper interfaces [5–8].

Wear and corrosion particles retrieved from tissues surrounding MoM devices have been shown to be predominantly in the nanometer-size range [4,9]; the particles are generally smaller than 50 nm (range 6–834 nm) with round or irregular morphologies. The wear particles have been generated in hip simulators to have similar size distribution and morphology as recorded clinically, however the *in vitro* studies so far have not established the mechanism behind the adverse local response to these wear products, such as aseptic chronic inflammation and pseudotumour formation [9–12], which is closely associated with pain and implant failure.

Prolonged inflammation results in ARMD at the implant site. First, wear particles and ionic corrosion products are detected and phagocytosed mainly by the tissue-resident macrophages [10] and if phagocytosed in a large number, these wear particles can activate macrophages to release an array of cytokines and chemokines to alarm circulating leucocytes [13]. Leukocytes infiltrating the inflamed tissue, promote recruitment of neutrophils or monocytes that differentiate locally into macrophages, and potentiate the pro-inflammatory environment. At the same time, the resolution of the inflammatory response occurs by removing the dead neutrophils and the egress of inflammatory macrophages from the inflamed tissue to the nearest opening of the draining lymphatics [14]. The undesired response to a MoM implant are frequently found to show soft tissue failure characterized by macrophage predominant infiltration with their massive intake of wear particles [15]. Metal ions (Co^{2+} and Cr^{3+}) have been shown to enhance the migration of T lymphocytes independently of circulating cytokines or chemokines resulting in an accumulation of T lymphocytes in the periprosthetic tissues of some patients with CoCr-based implants [16]. However, the mechanism behind the macrophage migration in the presence of both wear debris and ions is largely unknown.

This study aims to reveal the mechanism regulating macrophage migration during exposure to cobalt and chromium compounds, in order to understand the clinical manifestation of a chronic inflammatory response. We have shown that cobalt, but not chromium, affects the migration of macrophages through ROS and RhoA signalling pathways.

2. Materials and methods

2.1. Particles and ions

Cobalt and chromium nanoparticles were purchased from American Elements (Los Angeles, CA, USA). Cobalt nanoparticles (CoNPs) were composed of 90% cobalt and 10% cobalt (II,III) oxide with a molecular weight of 58.93 and had a diameter of 2–60 nm (data from the company). Chromium nanoparticles (CrNPs) were in the form of chromium oxide (Cr_2O_3) nanoparticles with a diameter of 10–30 nm (manufacturer data). Prior to use, the nanoparticles were washed in 100% ethanol for sterilisation and resuspended in sterile H_20 at a concentration of 1 mg/ml using a sonicator (pulsed mode, 3 min). Stock solutions (0.1 M) of Co^{2+} and Cr^{3+} ions were freshly prepared by dissolving $CoCl_2{\cdot}6H_2O$ (99.5% purity; Sigma Aldrich) and $CrCl_3{\cdot}6H_2O$ (98% purity; Sigma Aldrich) in sterile H_20. These solutions were sterilized by filtration through 0.2 μm pore size sterile syringe filter (Merck Millipore). Stock solutions of cobalt and chromium nanoparticles and ions were further diluted in cell culture medium to achieve the desired concentrations.

2.2. Characterization of the cobalt and chromium nanoparticles

Transmission Electron Microscopy (TEM; JEOL JEM-2010, Japan) was employed to observe the morphology of CoNPs and CrNPs as shown in Fig. S1. CoNPs and CrNPs were suspended in pure ethanol and a drop of particle suspension was placed onto the carbon coated grid. The polydispersity index (PDI) and the surface charge of cobalt and chromium nanoparticles in 1640 RPMI medium that were employed in this study were analysed by Zetasizer (Malvern Co., UK).

2.3. Cell lines and culture preparation

2.3.1. Human U937 monocytic cell line

Cells from the U937 cell line (passage 6-25, donation from Dr Akihisa Mitani, Imperial College London, UK) were cultured in RPMI 1640 medium (ThermoFisher, USA) supplemented with 10% FBS (Sigma, USA), 1.9 mM L-glutamine, 96 U/ml penicillin, 96 μg/ml streptomycin, 19 mM HEPES buffer, in a humidified atmosphere with 5% CO_2 at 37 °C. To induce differentiation into adherent macrophage-like cells, cells were treated with 50 ng/ml PMA (Phorbol 12-myristate 13-acetate, Sigma Aldrich) for 48 h and followed by rest for a further 24 h in complete RPMI 1640 medium prior to further experiments.

2.3.2. Isolation and differentiation of bone marrow-derived macrophages

Bone marrow-derived macrophages (BMDMs) were harvested, pooled and differentiated according to established standard protocols [17]. To review briefly, femurs and tibiae were obtained from 8 of 6–12-week-old C57BL/6 mice. All mice were cared for according to the UK Animal Scientific Procedures Act (1986) and by the Institutional Committee for Use and Care of Laboratory Animals. Experiments were performed under the UK Home Office Personal licence number I56EDA266 and the groups UK Home Office Project Licence number 70/7266. Bone marrow was flushed from femurs and tibiae and bone marrow cells were collected and differentiated in RPMI-1640 complete medium containing macrophage colony-stimulating factor (M-CSF, 50 ng/ml, R&D Systems, Minneapolis, MN, USA) for 7 days.

2.4. Cytotoxicity assay

A colourimetric assay, MTS, was performed to assess the effect of cobalt and chromium nanoparticles and ions on macrophage viability using the CellTiter 96® Aqueous One Solution Cell Proliferation Assay (Promega, Southampton, UK). Cells (U937 macrophages or BMDMs) were seeded at a concentration of 5×10^4 in 96-well plates. For vehicle control, cells were stimulated with complete RMPI medium. After incubation for 6 and 24 h, medium was aspirated and 100 μl of serum-free RPMI medium containing 10% MTS reagent was added to each well. Plates were subsequently incubated for 3 h at 37 °C and the absorbance was read at 490 nm using an Infinite F50 plate reader (Tecan, Switzerland). Five replicates of each exposure were tested and the entire assay was repeated for three separate experiments. The cell viability was determined as a percentage of control cell viability.

2.5. Cell motility and migration assays

2.5.1. Single cell motility monitoring

Macrophage migratory ability was first investigated using live cell imaging. Inverted microscope (Lumascope 720, Etaluma, USA) connected to a cell culture incubator was used for live cell imaging to visualise macrophage migration. Time-lapse images of migrating U937 macrophages at a seeded density of 2×10^4 cells/cm^2 in a 24-well plate were collected after 12 h incubation with Co^{2+} (200 μM), Cr^{3+} (400 μM), CoNPs (100 μM) or CrNPs (400 μM). The application of different concentrations of Co^{2+}, Cr^{3+}, CoNPs and CrNPs, Table 1, was based on the highest concentration that could be delivered whilst maintaining high cell viability, following cell viability tests shown in Fig. S2.

Images were captured every 5 min for 6 h. Migratory properties of individual cells identified from the time-lapse images were then analysed using ImageJ software (n = 25 cells/condition).

2.5.2. Transwell cell migration assay

Cell migration was also investigated using 6.5 mm Transwell chambers with 8 μm pores (Costar, Corning, NY, USA). Briefly, 2×10^5 harvested U937 macrophages or BMDMs in serum free RPMI 1640 medium were added to the upper chamber of the insert. The lower chamber was filled with 600 μl RPMI 1640 medium with 10% FBS to encourage cell migration down the FBS chemotactic gradient. Cells migration was analysed over a 6-hour period in the presence of Co^{2+} or Cr^{3+} that was added to both the upper and lower well at the required concentration or following 2-hour pretreatment with CoNPs or CrNPs (Table 1). After 6 h treatment, cells remaining on the membrane were fixed with 4% paraformaldehyde (Sigma, USA), stained with crystal violet (Sigma, USA) and counted.

2.5.3. In vivo macrophage migration assay and FACS (flow cytometry) analysis

To demonstrate the validity of the *in vitro* studies, the *in vivo* effect of cobalt ions on mouse macrophage migration was studied. 20 wt C57BL/6 mice were first injected intraperitoneally with 1 ml of 4% thioglycollate (Sigma, USA) to recruit macrophages into the peritoneal cavity. After 4 days, the mice were injected intraperitoneally with 5 μg of CoNPs (10 mice) or PBS (10 control mice). After 12 h, 5 mice from each group were injected with LPS (250 μl; 5 μg/ml) intraperitoneally to induce macrophages migration towards the regional lymph nodes; the remaining 5 mice from each group were injected intraperitoneally with PBS (250 μl) as blank control. After 4 h, the peritoneal cells were harvested by lavage and counted. The macrophages in the lavage were quantified by flow cytometry. Cell suspensions were pre-incubated with anti–CD16/CD32 mAb to block FcγRII/III receptors (BD Pharmingen) on ice for 15 min. After washing the suspension, cells were stained with PE/Cy5 anti-mouse CD11b antibody (Abcam, UK) and FITC anti-mouse F4/80 antibody (Abcam, UK). Stained cells were washed and re-suspended in 200 μl of PBS and analysed using a flow cytometer (BD ACCURI C6) and FlowJo software (TreeStar).

Table 1
Concentration of cobalt and chromium applied during the migration tests.

Treatment	Cell type	
	U937 macrophages	BMDMs
Co^{2+}	200 μM	50 μM
Cr^{3+}	400 μM	200 μM
CoNPs	100 μM	20 μM
CrNPs	400 μM	200 μM

2.6. Scanning electron microscope (SEM) analysis

U937 macrophages on the coverslips were fixed in 2.5% glutaraldehyde (Sigma, USA) for 2 h and dehydrated in graded ethanol (50%, 70%, 80%, 90%, 95%, and 100%; 10 min for each). The samples were transferred to critical-point drying with hexamethyldisilazane (Sigma, USA) then coated with a 5 nm thick layer of gold–palladium alloy. The SEM images were obtained with a scanning electron microscope (FEI Quanta 200) at a low voltage (~1 kV).

2.7. Immunofluorescence confocal and super resolution microscopy

Treated cells (U937 macrophages or BMDMs) were fixed with 4% paraformaldehyde (Sigma, USA) and washed and permeabilized with 0.5% Triton X-100 and rinsed 3 times with PBS. Nonspecific binding sites were blocked by adding PBS with 1% BSA. The adhesion protein, vinculin, was labelled by incubation at 4 °C, overnight with mouse monoclonal anti-vinculin primary antibody, clone hVIN-1 (1:400, Sigma, USA). Cells were then washed and incubated for 1 h at room temperature in Alexa 488 conjugated anti-Mouse IgG as Secondary Antibody (1:1000, Invitrogen, USA). In separate samples, cellular α-tubulin and acetylated α-tubulin were labelled using rabbit polyclonal anti-α tubulin antibody (1:200, Abcam, UK) and mouse anti-acetylated tubulin, clone 611B-1 (1:2000; Sigma-Aldrich, USA) respectively with Alexa 488 secondary antibodies as above.

To simultaneously label the F-actin, the samples were incubated for 30 mins with 200 μl of rhodamine-conjugated phalloidin (Molecular Probes, USA) in a humidified chamber at room temperature in the dark. Cell nuclei were stained by incubation with 5 μg/ml DAPI (Dojindo, USA) followed by two PBS rinses. Slides were then visualized with a fluorescence microscope (SP2, Leica, Germany) with ×63 objective. Slides were also imaged on a microscope (710 ELYRA PS.1, Zeiss, Germany) with a ×63/1.4NA objective for structural illumination microscopy.

2.8. Cell adhesion assay

U937 macrophages were seeded at a concentration of 2×10^5 cells/well into a 24-well plastic cell culture plate coated with 2% gelatin and treated with 100 μM, 200 μM or 300 μM Co^{2+}. After 30 min of incubation, cell culture medium in each well were aspirated and gently rinsed 2 times with warm PBS. Adherent cells of were then imaged (10 fields of each well were randomly selected) with an inverted microscope (DCF420, Leica, Germany) and counted.

2.9. Proteolytic activity measurement

2.9.1. In vitro ECM degradation assay

U937 macrophages were seeded onto coverslips coated with FITC-conjugated gelatin, as part of an *in vitro* ECM degradation assay, as previously described [18]. Briefly, glass coverslips were coated with 0.2 mg/ml FITC-gelatin (Molecular Probes, USA) in PBS and fixed with 0.5% glutaraldehyde, washed six times with PBS, then washed once with 70% ethanol/PBS and once with medium. U937 macrophages (1×10^5/well) were plated onto the coverslips and incubated at 37 °C in the presence of Co^{2+} (200 μM), CoNPs (100 μM), Cr^{3+} (400 μM) or CrNPs (400 μM) for 24 h, then fixed, processed for F-actin staining with rhodamine-conjugated phalloidin, and observed as described above. The coverslips were examined using a confocal microscope (SP2, Leica, Germany) and the total area that was degraded was measured using ImageJ software [18]. The matrix degradation index was calculated as the ratio between the area of gelatin matrix degraded by treated cells to that degraded by untreated cells.

2.9.2. Gelatin zymography

Conditioned media collected from cells treated by cobalt ions (100 μM, 200 μM, 300 μM) and nanoparticles (20 μM, 50 μM and 100 μM) for 24 h were used for gelatin zymography. The supernatants were subjected to electrophoresis in an 8% SDS-PAGE gel co-polymerized with gelatin (1 mg/ml, Sigma, USA). The gelatinolytic activities were detected as transparent bands against the background of Coomassie Brilliant Blue-stained gelatin and quantified using ImageJ software.

2.10. ROS measurements

ROS formation was measured using 5-(and 6-)-chloromethyl-2′7′-dichlorodihydrofluorescein diacetate (CM-H_2DCFDA, Life technologies, USA). Cells were cultured in black 96-well plates with a clear bottom. After exposure to cobalt, the supernatant was removed and cells were briefly washed with warmed PBS. CM-H_2DCFDA was dissolved in anhydrous DMSO to a final concentration of 1 mM and diluted further in Hank's balanced salt solution (HBSS, ThermoFisher, USA). Cells were exposed to 1 μM CM-H_2DCFDA for 30 min at 37 °C in the dark. Fluorescence was read at an excitation of 485/20 nm with emission 528/20 nm using a microplate reader (Synergy HT Multi-Mode, Biotek, USA).

2.11. Protein extraction and immunoblotting

All lysis buffers were supplemented with 1% protease inhibitor (Sigma Aldrich, USA). Protein extracts were resolved using gradient precast SDS – polyacrylamide gel electrophoresis (Biorad Laboratories Inc, USA), and then electro-transferred onto a nitrocellulose membrane by using Trans-Blot® Turbo™ Transfer System (Biorad Laboratories Inc, USA) for immunoblot analysis. Antibody probing was done as per manufacturers' instructions Antibodies used include anti-RhoA antibody (1:1000, Abcam, UK), anti-CDC42 antibody (1:1000, Abcam, UK), anti-Rac1 antibody (1:1000 Abcam, UK), anti-phospho-MYPT1 (Thr696) antibody (1:1000, Cell Signaling Technology, USA), anti-myosin light chain (phospho S20) antibody (1:1000, Abcam, UK), anti-GAPDH antibody (1:2000, Abcam, UK). Secondary antibodies either IRDye® 800CW Goat anti-Mouse IgG (LI-COR, USA) or IRDye® 800CW Goat anti-Rabbit IgG (LI-COR, USA) were used with dilution of 1:15000. Specific protein bands were detected using Odyssey® CLx Imaging System (LI-COR, USA).

2.12. Data analysis

All data are expressed as the mean ± SEM from independent repeat experiments (N = 3) unless otherwise stated. The number of repeat measurement per experiment (n) is indicated in each figure. All statistical differences were analysed with one-way ANOVA or Kruskal-Wallis test with Dunn's Multiple Comparison Test unless otherwise stated (SPSS Inc., Chicago, IL, USA). A value of $P < 0.05$ was considered statistically significant.

3. Results

3.1. Cobalt (II) ions and nanoparticles inhibit U937 macrophage random migration

To directly measure the impact of cobalt and chromium on macrophage motility *in vitro*, we first performed time-lapse imaging of U937 macrophages after 12 h of cobalt or chromium treatment using non-cytotoxic concentrations (Supplementary Fig. S2). Fig. 1A–E shows the migration paths for 25 individual cells in each treatment group. The total path length of cells treated with Co^{2+} and CoNPs were significantly shorter than those for untreated control cells ($P < 0.001$, Fig. 1F). Treatment with Cr^{3+} or CrNPs had no significant effect on macrophage migration.

3.2. Cobalt inhibits U937 macrophages and BMDMs transmigration

Using transwell migration assay we confirmed the results observed during random cell migration (Fig. 1). The ability of U937 macrophages to migrate through the porous transwell membrane was significantly impaired by pre-treatment with either Co^{2+} or CoNPs (Fig. 2). Exposure to Co^{2+} and CoNPs, reduced the number of transmigrating U937 macrophages by approximately 62% and 55%, respectively, whilst for BMDMs, the corresponding reductions in migration were approximately 45% and 53%, respectively (Fig. 2B). Incubation with Cr^{3+} and CrNPs had no statistically significant effect on the cell migration relative to untreated controls for either U937 macrophages or BMDMs.

3.3. CoNPs inhibit macrophage migration in vivo

To determine whether cobalt affects macrophage migration *in vivo*, we quantified the number of macrophages in the mouse peritoneal cavity before and after LPS stimulation in mice with or without cobalt pre-treatment. As neither Cr^{3+} nor CrNPs showed any significant effect on macrophage migration *in vitro*, only cobalt exposure was examined during the *in vivo* study. Mice were injected with cobalt nanoparticles to mimic the generated cobalt *in vivo* dissolution products. Harvested peritoneal macrophages were identified by a flow cytometry gating strategy according to their size and granularity (Fig. 3A), CD11b and F4/80 surface marker expression (Fig. 3B). In mice not stimulated with LPS, the CoNPs pre-treatment had no significant effect on the number of peritoneal macrophages compared with control group (PBS only). After LPS stimulation, a marked efflux of peritoneal macrophages (by approximately 60%, Fig. 3C) from the cavity of control mice (PBS only) was observed, consistent with previously published work [19]. In mice pre-treated with CoNPs, the LPS stimulation had no significant effect in inducing macrophages efflux, with the number of macrophages remained at similar levels to the CoNPs group without LPS treatment, which indicated that the ability of macrophages to migrate out of the peritoneal cavity was significantly inhibited by CoNPs.

3.4. Cobalt modulates microtubule acetylation in U937 macrophages

To initiate cell migration, internal forces developed by the actin cytoskeleton are transmitted through cell-substrate adhesion sites while a dynamic turnover of adhesion complexes occurs [20]. Disruption in the cell migration indicates either an alteration in this force transmission or changes in the cell adhesion strength. Uptake of metal particles can impede the force balance between the microtubule (MT) and F-actin by inhibiting MT polymerization in epithelial cells [21]. Therefore, we investigated whether microtubule or cytoskeletal impairment causes the inhibition of macrophage migration. The MT structure of the control and treated cells are shown in Fig. 4A. Both Co^{2+} and CoNPs induced a significant increase in U937 macrophage alpha tubulin acetylation, one of the basic components for MT biopolymer [22], confirmed by immunofluorescence staining (Fig. 4A and B) and Western Blot analysis (Fig. 4C and D). In contrast, chromium ions had no significant effect on the MT organisation or acetylation while CrNPs slightly reduced the MT acetylation, although it was not statistically significant. We also investigated the effect of an inhibitor of a member of the histone deacetylase family, HDAC6, which regulates MT-dependent cell motility via mediating tubulin deacetylation [23]. HDAC6 overexpression induces a global deacetylation of

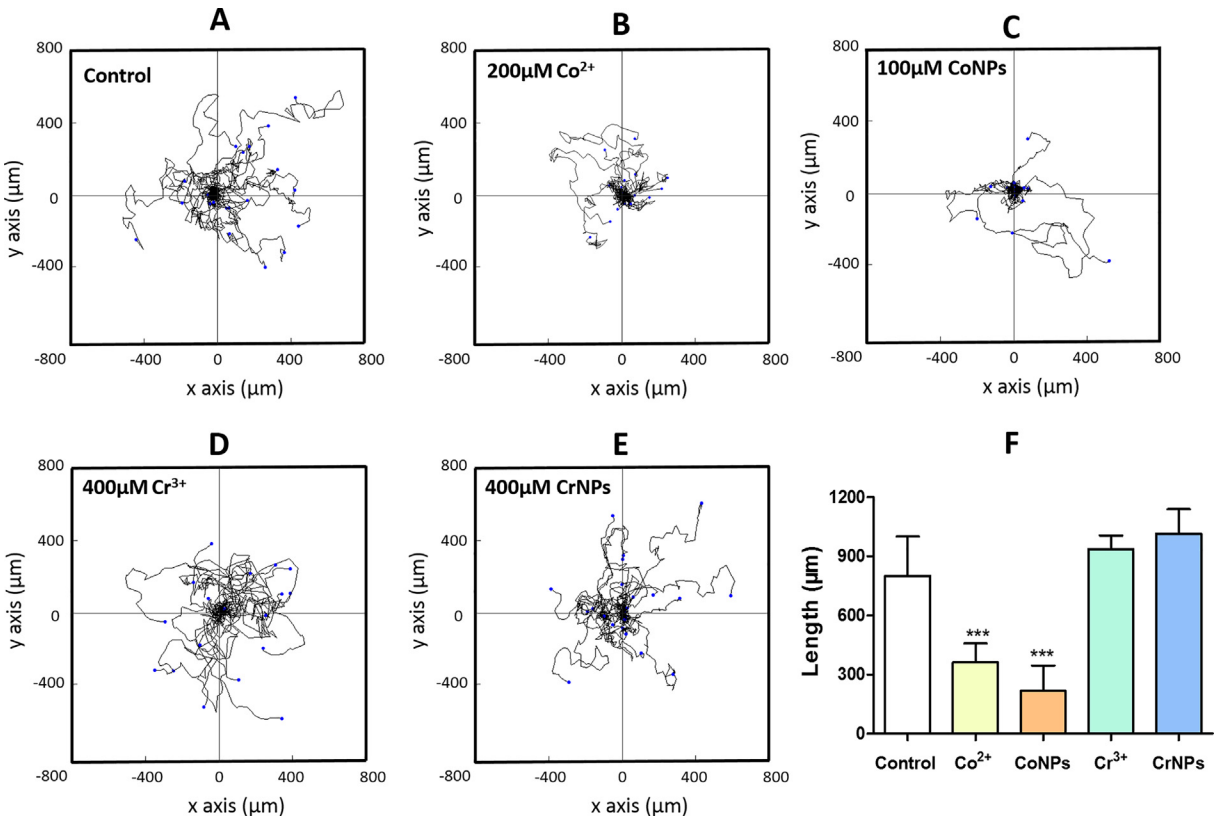

Fig. 1. Cobalt ions and nanoparticles reduce U937 macrophage random migration. (A-E): Detailed migration trajectories of cells (n = 25) over a 6-hour period following treatment with cobalt or chromium. Individual tracks were transposed so that each of the cells started at the same origin. (F) Net cell migration length for each treatment with values indicating mean + SEM for N = 3 experiments (n = 25 cells/condition/experiment). Statistical differences from untreated control are based on one-way ANOVA with Bonferroni post-test; $^{***}P < 0.001$.

α-tubulin, hence promoting cell chemotactic migration [23]. When U937 cell were treated with a HDAC6 inhibitor, Tubastatin A (5 μM), a hyperacetylation of tubulin was observed (Fig. 4A), showing much higher effect than the cobalt treatment. Tubastatin A also significantly reduced the number of migrating cells in a transwell migration assay, however only partially replicating the effect of cobalt treatment (Fig. 4E). This suggests that cobalt-mediated tubulin acetylation in macrophages does not play the critical role in the downregulation of cell migration.

3.5. Cobalt ions and nanoparticles promote macrophage spreading and podosome formation, which are associated with increased cell adhesion

Macrophage migration involves remodelling of the actin cytoskeleton associated with cell spreading, disassembly of existing focal adhesions, and formation of new cell-matrix interactions. SEM imaging revealed that both Co^{2+} and CoNPs significantly increased U937 macrophage spreading with increase in lamellipodia protrusions around the cell periphery (Fig. 5A). In this case, CoNP-treatment had a significantly greater effect than Co^{2+} treatment (Fig. 5B). U937 macrophages expressed characteristic podosome-like punctate adhesion structures, characterised by an actin-rich core surrounded by vinculin adhesion proteins (Fig. 5C). Treatment with either Co^{2+} or CoNPs significantly increased both the podosome number (Fig. 5D) and density within individual cells (Fig. 5E). Cobalt also significantly increased the percentages of cells forming podosomes in BMDMs (Fig. S4). Excessive formation of the adhesion complex can result in a strong anchorage of cells to the underlying substrate, thereby inhibiting cell migration [24]. Hence, we examined whether changes in macrophage morphology and podosome formation during cobalt treatment were associated with alterations in cell adhesion. U937 cells exposed to Co^{2+} showed an increased cell adhesion to the ECM in a concentration-dependent manner (Fig. 5F and G). This effect of Co^{2+} was not evident on BMDMs (data not shown), possibly due to differences in the speed of the cell adhesion to the matrix. Collectively, these results indicate that the cobalt-induced inhibition of macrophage migration is associated with cytoskeletal reorganisation, podosomes formation and increased cell adhesion.

3.6. Cobalt-induced podosome formation in U937 macrophages stimulates ECM degradation

Podosomes promote adhesion to the substrate and degrade the components of the ECM. To determine whether cobalt-induced podosomes are able to locally degrade the ECM, we performed an *in vitro* matrix degradation assay based on loss of FITC-conjugated gelatin. Macrophages induced localised degradation as shown by dark areas in the fluorescent-tagged gelatin matrix (indicated by arrows in Fig. 6A). The degradation of gelatin was closely associated with cells expressing podosomes and in some cases, the podosomes were located directly over the degraded matrix (Fig. 6A). Both Co^{2+} and CoNPs promoted matrix degradation (Fig. 6B), with associated statistically significant differences in matrix degradation index (Fig. 6C). Treatment with Cr^{3+} and CrNPs had no significant effect on the ECM degradation (Fig. 6B).

The matrix degradation by podosomes involves the recruitment and activation of matrix metalloproteinases (MMPs) [25]. Using a zymography assay we measured the release and activation of MMPs. We observed release of MMP9 (band at a molecular weight of 82–92 kDa) after cobalt treatment (Fig. 6D). Additionally, a lower band of 82 kDa molecular weight was observed indicating

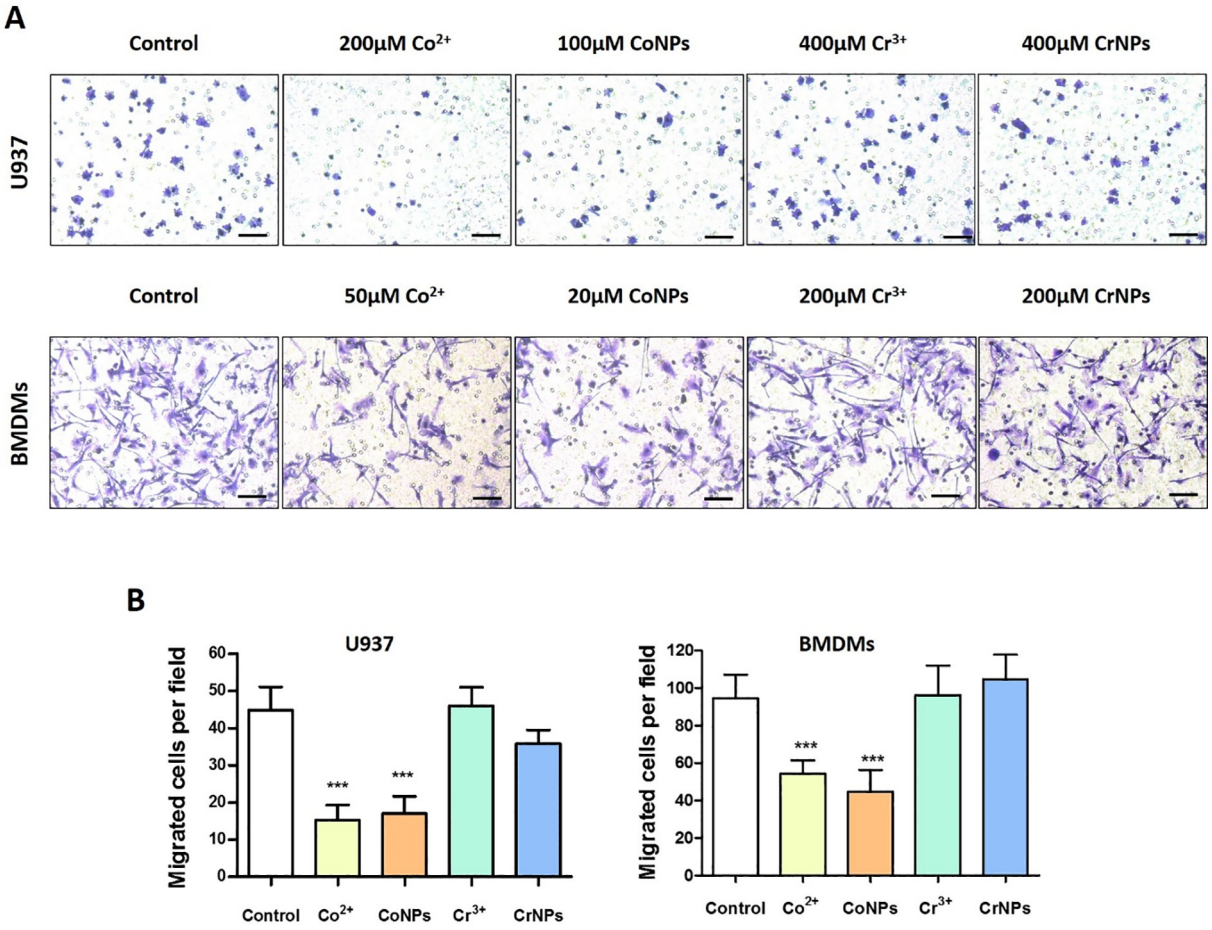

Fig. 2. Cobalt ions and nanoparticles reduce transmigration of U937 macrophages and BMDMs. (A) Representative images of migrated U937 macrophages and BMDMs treated by Co^{2+}, CoNPs, Cr^{3+} and CrNPs (Scale bar = 100 μm). (B) Quantifications of the migration assay based on three independent experiments. Values represent mean ± SEM. N = 3. For each experiment, 10 random fields were imaged for each treatment (n = 10). Statistically significant differences are indicated relative to untreated control based on one-way ANOVA with Bonferroni post-test; $^{***}P < 0.001$.

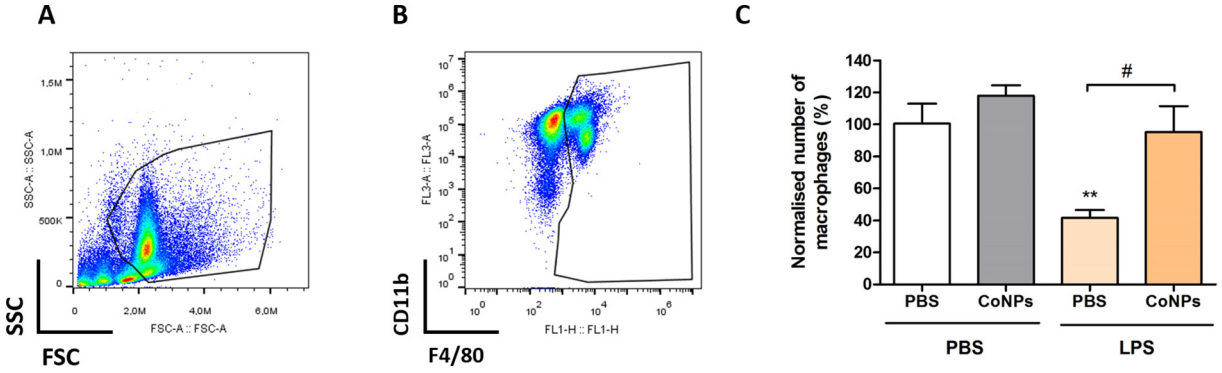

Fig. 3. Macrophage migration *in vivo* is inhibited by CoNPs. Representative FACS analysis images showing the gating strategy to identify the peritoneal macrophages based on (A) cell size and granularity, (B) CD11b and F4/80 surface markers expression. (C) Number of harvested macrophages from treated mice from each group, with data normalised to PBS control group (mice injected with PBS twice). Statistically significant differences were determined by one-way ANOVA and Bonferroni's multiple comparison test (n = 5 mice per treatment, **indicates difference from PBS control (PBS only) $P \leq 0.01$; # indicates difference between CoNPs and PBS treatment with LPS, $P < 0.05$).

an active form of MMP9 cleaved from pro-MMP9. Co^{2+} and CoNPs induced pro-MMP9 release was not concentration-dependent, while the formation of active MMP9 was (Fig. 6E). Cobalt exposure had no significant effect on MMP2 release. Immunofluorescent staining revealed that intracellular MMP9 frequently co-localised with cobalt-induced podosomes (Fig. S3). In line with the results shown in Fig. 6B, Cr^{3+} and CrNPs did not cause any significant change in the release of MMP2, pro-MMP9 nor the active form of MMP9 (data not shown).

3.7. Inhibition of macrophage migration in the presence of cobalt was associated with ROS production and its down-regulation of RhoA expression.

Heavy metal ions and nanoparticles can provoke cellular stress, which may lead to alterations in cellular structure and function, and potentially loss of cell viability [26]. Both Co^{2+} and CoNPs induced ROS in a concentration-depended manner in U937 macrophages, and we showed that this also occurs at non-cytotoxic

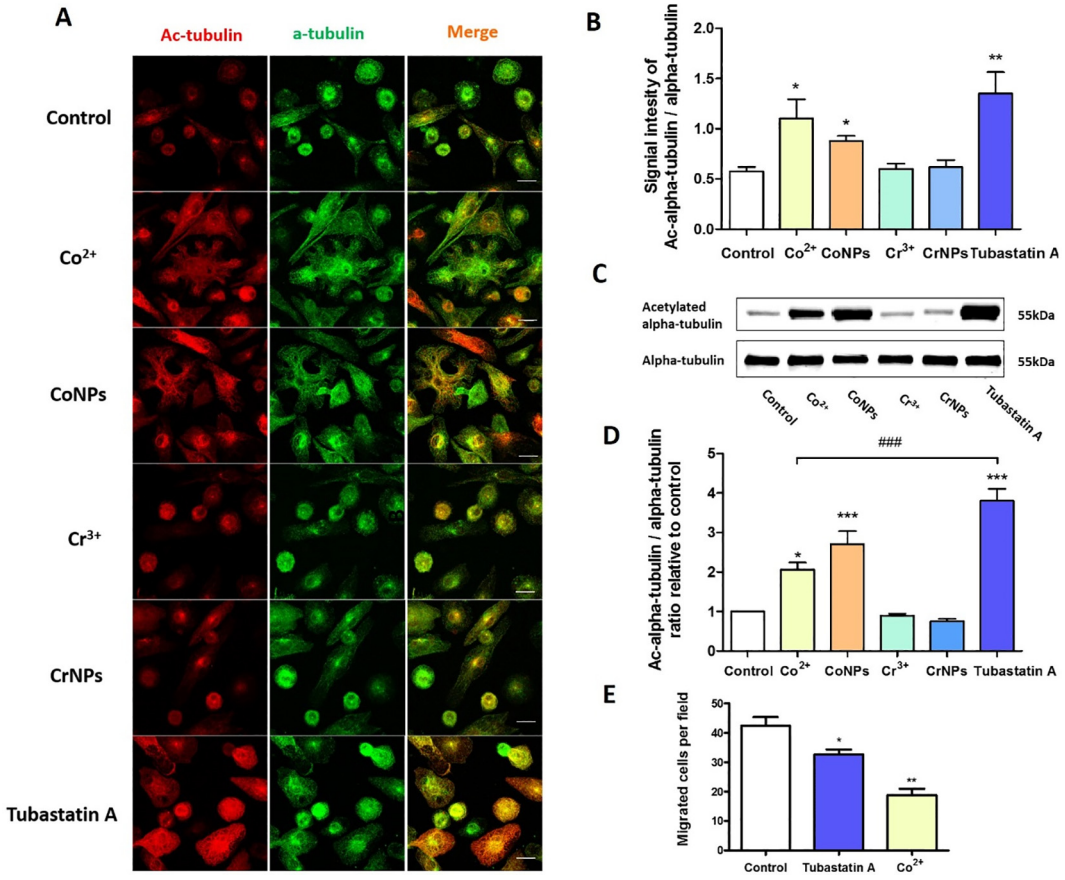

Fig. 4. Cobalt-induced hyper-acetylation of tubulin and its effect on macrophage migration. (A) Representative immunofluorescence confocal images of U937 macrophages treated with Co^{2+}, CoNPs, Cr^{3+}, CrNPs and Tubastatin A for 24 h. Cells were stained for acetylated α-tubulin (red) and α-tubulin (green). Scale bar represents 20 μm. Integrated fluorescent signal intensity for acetylated and non-acetylated tubulin in each cell was quantified and shown in (B) n = 25; values represent mean + SEM; $^{*}P \leq 0.05$; $^{**}P \leq 0.01$; N = 3. (C) Western blots for acetylated α-tubulin and α-tubulin for cells treated with cobalt, chromium, Tubastatin A for 24 h and (D) the corresponding quantification demonstrating increased total α-tubulin acetylation. Values represent mean + SEM; $^{*}/^{***}$ indicate difference from control, $P \leq 0.05/P \leq 0.001$; $^{\#\#\#}$ indicates difference between Co^{2+} and Tubastatin A, $P \leq 0.001$; N = 3. (E) Increased tubulin acetylation with Tubastatin A significantly reduced macrophage transwell migration. Values represent mean + SEM; $^{*}P < 0.05$, $^{**}P \leq 0.01$; N = 3 experiments, n = 10 fields of view per experiment. All statistically significant differences were determined by one-way ANOVA and Bonferroni's multiple comparison test. (For interpretation of the references to colour in this figure legend, the reader is referred to the web version of this article.)

concentrations (Fig. 7A). The maximum increase in ROS production of approximately 90% compared to unstimulated cells, occurred within the first 30 min. This significant increase persisted for 4 h of treatment but decreased after 6 h. Exposure to CoNPs at 100–1 50 μM induced a transient upregulation in ROS measured at 2 h, with an increase of approximately 75% at 150 μM (Fig. 7B). Co-treatment with ROS scavenger and antioxidant, NAC (N-acetyl-L-cysteine), abolished the cobalt-induced ROS production in cells (Fig. 7A and B). We next tested whether ROS generation was responsible for the cobalt-induced podosome formation and the consequent inhibition of U937 macrophage migration. Co-treatment of Co^{2+}-treated cells with NAC resulted in a reduction in the cobalt-induced podosome formation (Fig. 7C and D) and a significant increase in Co^{2+}-treated macrophage transmigration (Fig. 7E). As mitochondria and NADPH oxidases are the main sources of cellular ROS, we also tested the effect of a NADPH oxidase inhibitor apocynin (5 μM, 10 μM and 50 μM). However, apocynin was not able to inhibit cobalt-mediated ROS generation nor to restore macrophage migration (data not shown), which suggested that cobalt-mediated ROS increases are mainly mitochondria-derived.

Actin organisation and podosome turnover are tightly regulated by the Rho GTPase, such as RhoA, Rac1 and Cdc42, whose activity is determined by their guanine nucleotide-bound state [27]. To determine if cobalt-induced ROS acts as an upstream regulator to activate Rho GTPases, we investigated the expression of RhoA, Cdc42 and Rac1 after U937 macrophages were treated by Co^{2+} (200 μM) and CoNPs (100 μM) for 24 h. As shown in Fig. 7F and G, cobalt did not affect the Rac1 and Cdc42 levels, but caused decreased RhoA expression indicating that Co^{2+} and CoNPs negatively regulate RhoA signalling. This was further confirmed by down-regulation of the downstream proteins of RhoA signalling, such as pMLC (phospho-myosin Light Chain) and pMYPT (phospho-myosin-binding subunit of myosin phosphatase).

In addition, the treatment of macrophages with the RhoA-specific inhibitor C3 Transferase (2 μg/ml) and RhoA/ROCK1 pathway inhibitor Y-27632 (20 μM) also led to intensive cell spreading and increased podosome formation (Fig. 7H) as observed in cobalt-treated cells. Accordingly, the migration of U937 macrophages were also significantly impaired when RhoA signalling was inhibited by inhibitor C3 Transferase and Y-27632 (Fig. 7H and I). Furthermore, the reduced expression of RhoA level caused by Co^{2+} and CoNPs was significantly reversed by using the NAC (Fig. 7 J and K), which has showed to suppress the cobalt-induced ROS generation and be capable of partially restore the migration ability of U937 macrophages. These data suggest that cobalt-induced ROS production lies upstream of the RhoA signalling and down-regulation of RhoA expression results in remodelling of macrophage cytoskeleton and impaired migration.

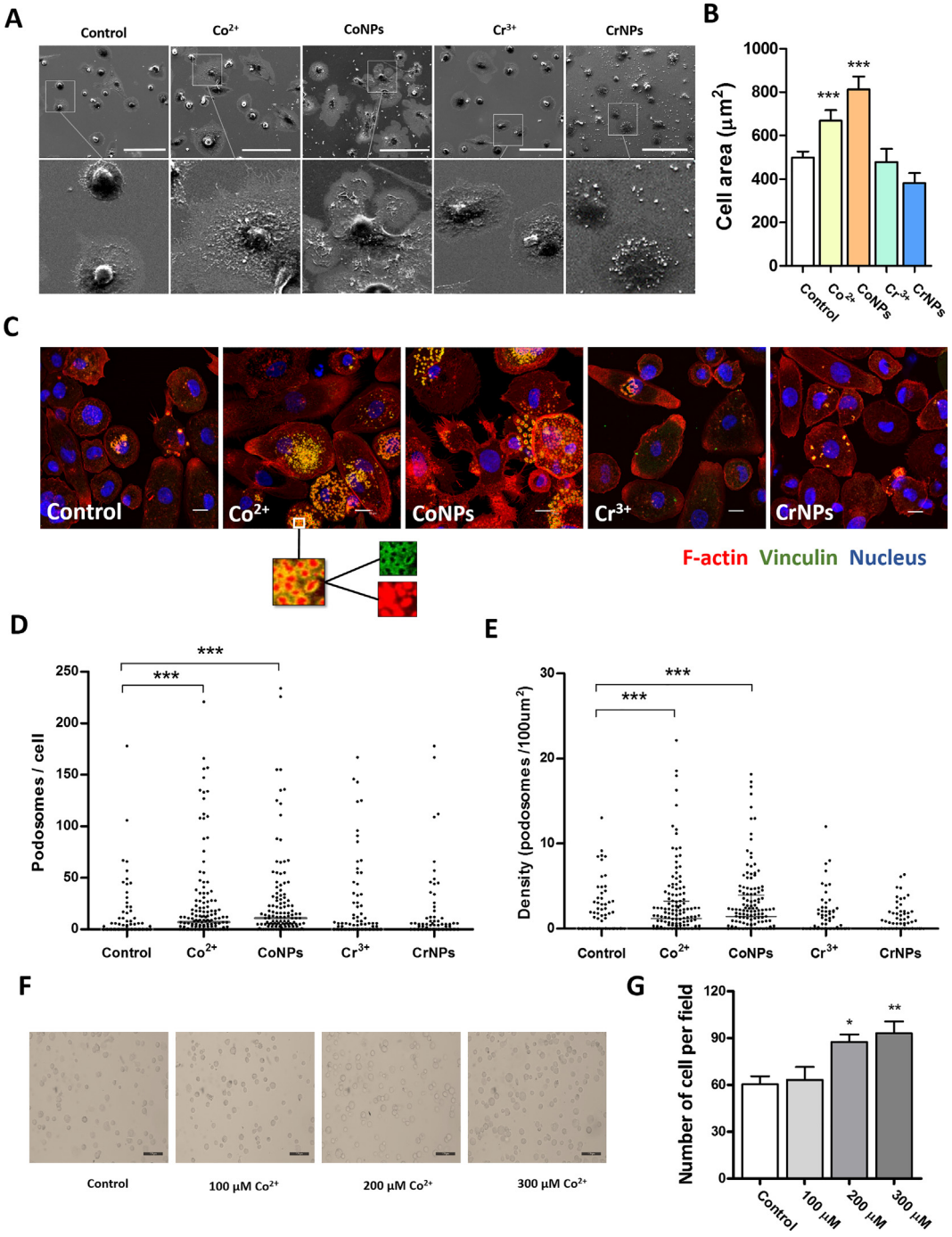

Fig. 5. Reduced macrophage migration induced by cobalt is associated with increased cell spreading and podosome formation and cell adhesion to extracellular matrix. (A) Representative SEM images of U937 macrophages incubated for 12 h with Co^{2+} (200 μM), CoNPs (100 μM), Cr^{3+} (400 μM) or CrNPs (400 μM) and untreated control. Scale bar indicates 100 μm. (B) Quantification of projected cell area for each treatment. Values represent mean + SEM for N = 3 separate experiments with n = 150 cells per experiment. Statistically significant differences from untreated control determined by one-way ANOVA and Bonferroni's multiple comparison test. $^{***}P \leq 0.001$. (C) Representative confocal microscopy images showing appearance of punctate podosome adhesion structures consisting of actin core (red) and surrounded by vinculin (green) in U937 macrophages following treatment with cobalt or chromium as described in (A). Scale bar indicates 10 μm. Associated quantification of (D) podosome number/cell and (E) podosome density. n = 150 cells for each group. Data with median shown from one representative experiment out of three; significance was determined by Kruskal-Wallis test and Dunn's Multiple Comparison Test. $^{***}P \leq 0.001$; N = 3. (F) Representative brightfield fields of view images showing that cobalt increased cell adhesion to ECM in a dose-dependent manner, where the scale bar indicates 100 μm, as quantified in (G) showing significantly increased numbers of adherent cells per field of view at 200 μM and 300 μM. Data indicates mean + SEM for N = 3 with n = 10 fields of view per experiment. Statistical significance based on one way ANOVA and Bonferroni's multiple comparison test; $^{*}P \leq 0.05$, $^{**}P \leq 0.01$. (For interpretation of the references to colour in this figure legend, the reader is referred to the web version of this article.)

4. Discussion

Macrophages play an essential role in surveillance and coordination of the inflammatory cascade associated with implant stability. The production of CoCr alloy wear debris leads to phagocytosis of the particles by macrophages [28]. This metal debris with associated ions activate the monocyte/macrophage lineage to release a variety of mediators, such as free radicals, nitric oxide, tumour necrosis factor-α (TNF-α), interleukin-1 β (IL-1 β), prostaglandin E2 (PGE2) and IL-6 [29–32], which are influenced by the

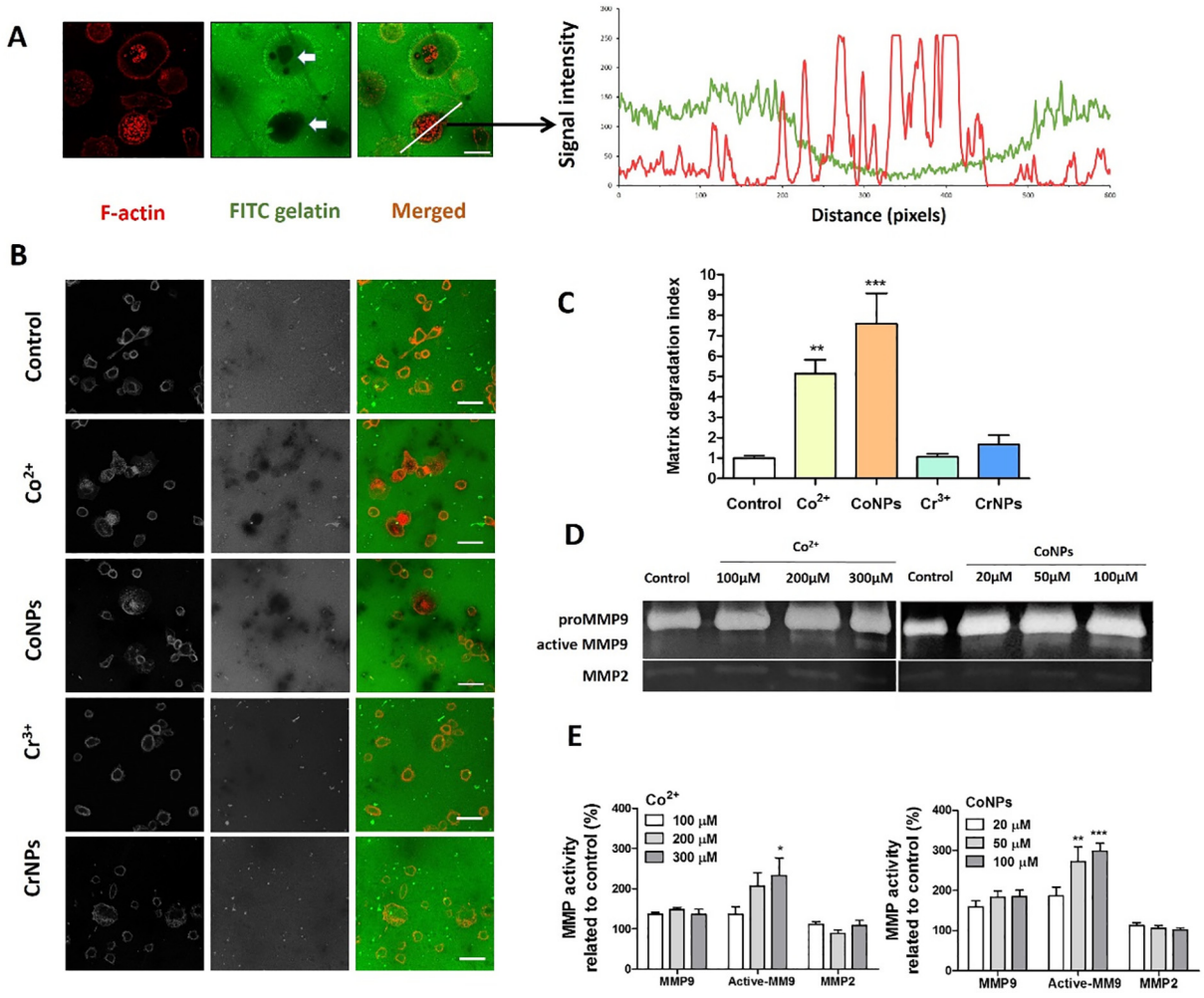

Fig. 6. Enhanced ECM degradation induced by cobalt is associated with the release and activation of MMP9, which co-localizes with podosomes. (A) Representative fluorescence microscopy image showing FITC-conjugated gelatin (green) degraded by U937 macrophages counter stained for F-actin (red) podosomes. Associated fluorescence intensity measurements demonstrate the co-localization of areas of gelatin degradation and the F-actin podosomes. Scale bar indicates 10 μm. (B) Representative images showing FITC-conjugated gelatin degradation following 24 h treatment with Co^{2+} (200 μM), CoNPs (100 μM), Cr^{3+} (400 μM) or CrNPs (400 μM) and untreated control. Scale bar indicates 20 μm. (C) Associated measurements of degradation area quantified as degradation index normalized to control group show significantly increased degradation following cobalt treatments. Values represent mean + SEM for N = 3 with n = 10 fields of view per experiment. (D) Zymography gels showing the release and activation of MMP9 by U937 cells due to cobalt treatment. (E) Quantification of the formation of pro-MMP9, active MMP9 and MMP2 based on gelatin zymography results, values represent mean + SEM for N = 5. All statistically significant differences between different groups and control were determined by one way ANOVA and Bonferroni's multiple comparison test; $^{*}P \leq 0.05$, $^{**}P \leq 0.01$, $^{***}P \leq 0.001$. (For interpretation of the references to colour in this figure legend, the reader is referred to the web version of this article.)

concentrations, shape and size of the particles [4]. Metal debris and ions can sensitize the immune system by inducing a delayed type IV hypersensitivity response [33]. Moreover, CoCr nanoparticles have been shown to be able to induce DNA damage and chromosomal aberration across cellular barriers [34]. In our study we elucidated the mechanism of altered macrophage behaviour by metal ions and particles at non-cytotoxic concentrations.

We used a combined *in vitro* and *in vivo* approach to examine the differential response of macrophages to cobalt and chromium ions and nanoparticles. Using a range of techniques, we have demonstrated for the first time that non-toxic levels of cobalt significantly reduce macrophage migration due to impaired egress capacity of macrophages. We have also further elucidated the underpinning molecular mechanism, which involves down-regulation of RhoA expression through induced ROS production. These findings provide new mechanistic explanation of the extensive clinical failures of orthopaedic implants manufactured from CoCr alloys, which are associated with retention of the macrophages and consequent prolonged and unrestrained inflammatory reactions that could lead to implant failure ultimately. In particular, the present *in vitro* results revealed that relatively low levels of both Co^{2+} ions (100 μM) and CoNPs (200 μM) markedly inhibit the random migration and chemotaxis of both U937 macrophages and murine bone marrow derived macrophages (BMDM), while Cr^{3+} and CrNPs demonstrated no significant effect (Figs. 1 and 2). This was confirmed in an *in vivo* peritoneal macrophage efflux experiment, where we found that CoNPs inhibit the macrophage emigration from the cavity triggered by LPS (Fig. 3).

The mechanisms of the particulate-mediated inflammatory response associated with the imbalance in tissue homeostasis remain unclear, although a retention of macrophages within periprosthetic tissues is often reported [35,36]. We report, for the first time, that the retention of macrophages during cobalt exposure is associated with an increase in both podosome formation and cell spreading (Fig. 5). These morphological and structural changes associated with macrophage retention are dependent on ROS formation (Fig. 7). Additionally, during increased podosome formation, an increase in MMP9 production occurs, resulting in a

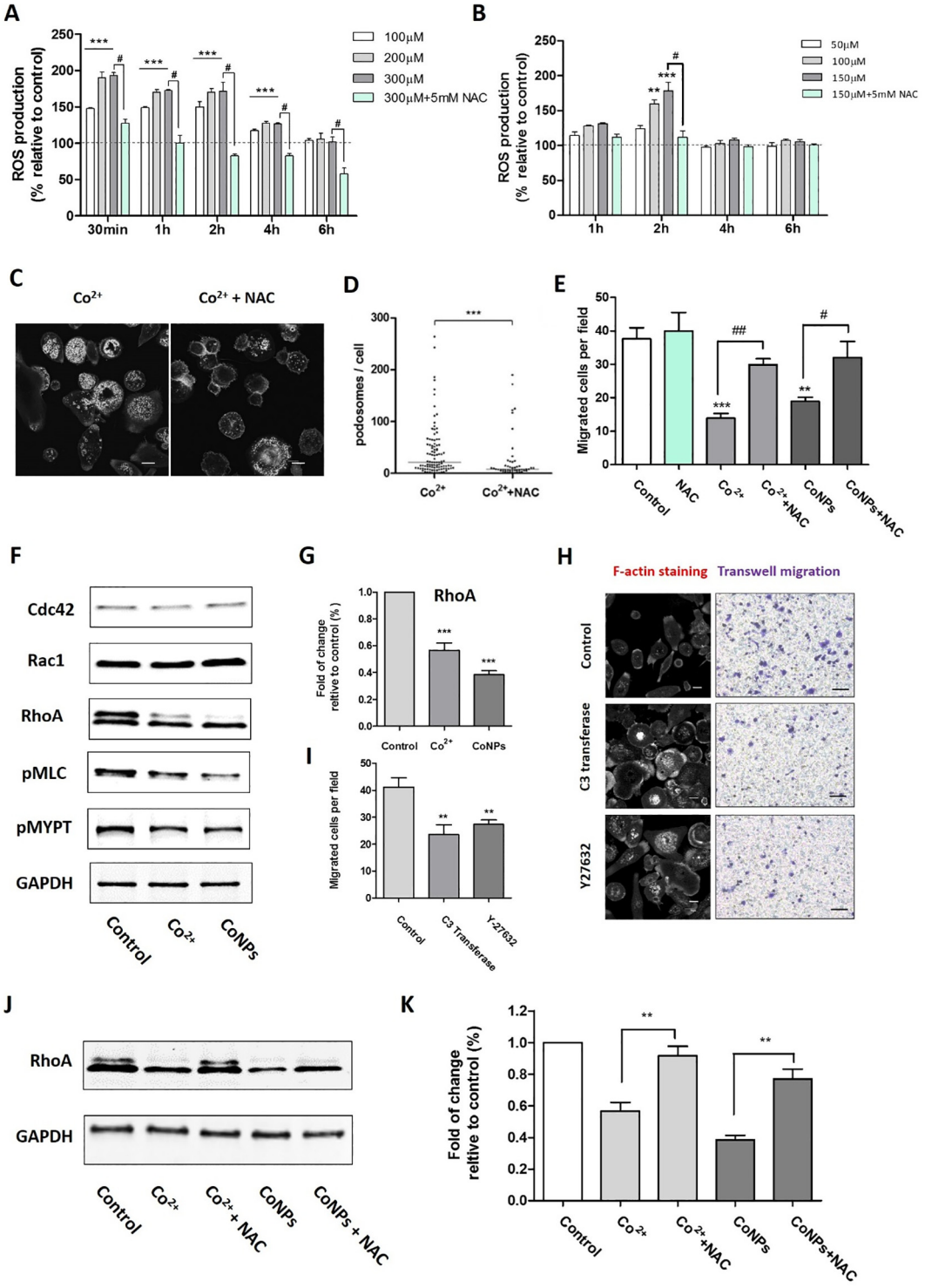

Fig. 7. Cobalt stimulates ROS production which stimulates podosome formation and impedes macrophage migration. (A, B) Dose and time dependent ROS production induced by Co^{2+} and CoNPs; values represent mean + SEM from N = 3 separate experiments. Statistically significant differences determined by one-way ANOVA and Bonferroni's multiple comparison test. ($^{**}P \leq 0.01$; $^{***}P \leq 0.001$, (***indicates significant upregulation for all of the three concentrations). (C) Fluorescence images showing that the ROS inhibitor, NAC (5 mM, 12 h) prevents Co^{2+} induced upregulation of podosome formation as shown by F-actin labelling with phalloidin and quantified in (D), data with median shown from one representative experiment out of three; significance was determined by Mann-Whitney test. $^{***}P \leq 0.001$; N = 3. (E) Suppression of U937 macrophage transmigration is rescued by treatment with NAC. Data indicates the mean + SEM for number of migrated cells per field of view from 3 separate experiments, N = 3, with n = 10 fields of view per experiment ($^{\#}P \leq 0.05$, ##/$^{**}P \leq 0.01$; $^{\#\#\#}$/$^{***}P \leq 0.001$). Scale bars represents 10 μm. (F) Western blots results for untreated cell and cells treated with Co^{2+} (200 μM) and CoNPs (100 μM) for 24 h. (G) The corresponding quantification demonstrating decreased RhoA expression. Values represent mean + SEM; ***indicate difference from control, P < 0.001; N = 3. (H) Representative images showing the effects of inhibitor C3 Transferase and Y-27632 on U937 macrophage cytoskeleton organization and migration. (I) Quantification of the effects of C3 Transferase and Y-27632 on U937 macrophage organization. Values represent mean ± SEM. N = 3. For each experiment, 10 random fields were imaged for each treatment (n = 10). $^{**}P < 0.01$. (J) Western blots results showing RhoA level reduced by Co^{2+} and CoNPs could be partially restored by inhibition of ROS with NAC (5 mM). (K) The corresponding quantification of cellular RhoA level with treatment by Co^{2+}, CoNPs and NAC. Values represent mean + SEM; **indicate difference from control, P < 0.01; N = 3. Scale bars represents 10 μm in (C) and (H).

greater matrix degradation, all driven in a cobalt concentration-dependant manner (Fig. 6). This mechanism reducing macrophage migration in response to Co^{2+} ions and CoNPs provide a new insight into the tissue responses and subsequent implant failure assocaited with CoCr alloys.

The mechanism of cell migration is controlled by a co-ordinated turnover of the actin and microtubule cytoskeletal network [37]. Migration is regulated by actin polymerization with actin/myosin interactions forming contractile forces to retract the cell, while microtubules specify migration directionality [38]. When studying the effect of cobalt and chromium on these critical components of the cell migration machinery, we observed a slightly decrease in the acetylation of α-tubulin in response to CrNPs, without affecting cell motility (Figs. 4 and 2). In contrast, cobalt increased α-tubulin acetylation while inhibiting cell migration. To test whether increased acetylation initiates the inhibition of macrophage migration, we induced tubulin acetylation with Tubastatin A, a potent HDAC6 inhibitor [22]. Tubastatin A treatment resulted in higher levels of α-tubulin acetylation than cobalt, and a reduction in macrophage migration, but to a smaller extend than cobalt (Fig. 4E). These results indicate either a non-specificity of Tubastatin A or that the migration response to cobalt involves additional mechanisms.

Apart from tubulin modifications, we found that cobalt induced alteration in macrophage morphology by enhancing cell spreading and an increase in the number and density of podosomes (Fig. 5A and D). Both cell spreading and podosomes formation involve the deformation of a cell membrane and the strengthening of cell–substrate attachment [39,40]. Podosome-type adhesions are rich in vinculin and other types of adhesion proteins, and regulate cell adhesion to the ECM [40]. Cell spreading and short-lived podosome formations with their adhesion structures are associated with enhanced macrophage migration and invasion [27]. When either process is uncontrolled, cell migration can be hindered [41]. For example, the inflammatory mediator PGE2 promotes macrophage migration in response to chemotactic signals, but at high doses, it reduces macrophage chemotaxis by enhancing cell-substratum adhesion [24]. In our study, we confirmed that the non-toxic concentrations of Co^{2+} led to a concentration-dependent increase in cell adhesion to the ECM substrate (Fig. 5F and G). These results suggest that the reduction in macrophage migration induced by cobalt is due to both the increased cell spreading and the enhanced podosome formation.

We also found that the molecular mechanisms through which cobalt regulated podosome adhesion and reduced migration, involves the formation of ROS (Fig. 7). Both Co^{2+} and CoNPs were shown to promote generation of the oxidative stress and increase ROS levels *in vitro* [42,43]. ROS is generated as a by-product during cellular oxidative metabolism, although its overproduction enhances cellular oxidative stress, transforming cells so they are unable to maintain normal physiological functions [44,45]. ROS are also the key signalling molecules during the progression of inflammatory disorders [46], by modulating the production of inflammatory chemokines and expression of leukocyte adhesion receptors to accumulate circulating monocytes at affected sites [46]. Oxygen radicals produced by local macrophages may further facilitate macrophage accumulation and their activation, resulting in prolonged inflammation. Our findings indicate that the mechanism behind the retention of infiltrated macrophages at the inflamed sites is mediated by ROS through regulating the cytoskeleton reorganization.

The cytoskeleton reorganization in presence of ROS is driven by the ability of ROS to induce reversible oxidation of proteins, which involves direct modification of protein kinases and transcription factors [47]. Major regulators of macrophage motility and cytoskeleton organization are influenced by Rho family GTPase [48–50], F-actin regulation pathways [51] and tyrosine phosphorylation [52,53]. The Rho family of GTPases play critical roles in cell motility by affecting actin organization and microtubule dynamics, myosin activity, and cell–ECM and cell–cell interactions [54]. In this study, we showed for the first time that cobalt-induced ROS formation acts as an upstream regulator to directly inactivate the RhoA, leading to reorganization of macrophage cytoskeleton and impaired cell migration (Fig. 7F–K). Small GTPase Rho is known to stimulate stress fiber formation and hamper the cell migration in many types of cells [55]. It is even reported that inactivation of Rho in transformed fibroblasts by dominant negative RhoA or the C3 exoenzyme would disrupt podosome structure [56], but also that podosome formation in Src-transformed fibroblasts could be promoted by limiting Rho activation [57]. In addition, it was recently revealed that podosome disassembly is associated with the activation of Rho and blockade of RhoA signalling could promote actin core assembly and podosome formation in macrophages [58].

Underlying mechanisms through which biomaterials-induced ROS formation modulates macrophage behaviour are of considerable importance. Despite emerging advances in materials science, biomaterials do not behave like native biological components and frequently incite adverse tissue reactions, which may lead to ultimate failure of the implants. Therefore accurate and facile approaches for screening and evaluating the biocompatibility of biomaterials are of critical interest, especially understanding the cellular behaviour of macrophages because of their decisive role in the long term survival of implanted biomaterials in addition to orchestrating inflammatory processes.

Over recent years, the use of MoM total hip replacement is in a drastic decline due to CoCr-related issues. However, implants containing CoCr alloys are still being widely utilized, such as in dental prosthesis and modular heads in MoP couplings. Significant increase in the amount of metal ion released into the saliva of patients with dental metallic materials has been reported [59]. Modular taper junctions allow for patient-specific fitting of implants. However, numerous retrieval studies have recently documented the adverse tissue reactions and pseudotumor formation adjacent to taper junctions in hip implants [5,7], which are clinically and histologically similar to ALTRs previously seen in failed MoM bearing. The etiology of this soft-tissue damage is also linked to release of metal ions and debris from the modular taper junctions. Therefore, further investigation is required to elucidate these different, yet similar, exposure scenarios. More importantly, a comprehensive biological evaluation of metal exposure is necessary due to the potentially destructive nature of these adverse reactions.

We acknowledge several limitations in this study. Although we have provided an explicit demonstration of the effect of cobalt on macrophage migration behaviour via a range of *in vivo* and *in vitro* techniques, it is still unknown whether macrophage accumulation around MoM hips is caused by a defective migratory ability. A refined animal study with *in vivo* tracking of macrophage recruitment would facilitate further investigation and yield improved understanding. Using commercially available nanoparticles in place of cobalt and chromium wear debris allowed us to decipher the individual role of the two primary elements in the cellular response. Possible synergistic effect of these two metals is of importance and should be addressed in the future studies. Both human U937 cell line and primary murine macrophages were used for data consistency, instead of primary human macrophages. These cellular models excluded the influence of variability in cells from different human donors, as have been used as *in vitro* cell models to study responses to orthopaedic wear products including bone cement, polyethylene, ceramic, metal particles, as well as metal ions [32,60–62]. Findings of our current study, can help us

design further investigations using primary human cells to characterize individual patient's responses to the wear debris.

5. Conclusion

Our study identified a new downstream effect of cobalt-induced ROS production and reduced RhoA expression in modulating macrophage migration and cytoskeleton organization. The effects of this signalling cascade lead to an enhancement in macrophage spreading, adhesion and inhibition of migration, which could induce a prolonged immune cell retention thereby propagating the chronic inflammation. The increased podosome formation in macrophages is also associated with enhanced activation of MMP9 and associated increased matrix degradation. The identification of this new mechanism through which cobalt, but not chromium, ions and nanoparticles induce macrophage retention at inflammatory sites provides a novel insight into the metal-associated periprosthetic tissue lesions.

6. Acknowledgement

The authors are grateful to the China Scholarship Council (CSC) for the support of Jing Xu.

Appendix A. Supplementary data

Supplementary data associated with this article can be found, in the online version, at https://doi.org/10.1016/j.actbio.2018.03.054.

References

[1] W.a.N.I. National Joint Registry for England, 13rd annual report, 2016, (2016).
[2] Y.M. Kwon, A.V. Lombardi, J.J. Jacobs, T.K. Fehring, C.G. Lewis, M.E. Cabanela, Risk stratification algorithm for management of patients with metal-on-metal hip arthroplasty: consensus statement of the American Association of Hip and Knee Surgeons, the American Academy of Orthopaedic Surgeons, and the Hip Society, J. Bone Joint. Surg. Am. 96 (1) (2014) e4.
[3] M.E. Muller, The benefits of metal-on-metal total hip replacements, Clin. Orthop. Relat. Res. 311 (1995) 54–59.
[4] A.K. Madl, M. Kovochich, M. Liong, B.L. Finley, D.J. Paustenbach, G. Oberdorster, Toxicology of wear particles of cobalt-chromium alloy metal-on-metal hip implants Part II: Importance of physicochemical properties and dose in animal and in vitro studies as a basis for risk assessment, Nanomedicine 11 (5) (2015) 1285–1298.
[5] D.R. Plummer, R.A. Berger, W.G. Paprosky, S.M. Sporer, J.J. Jacobs, C.J. Della Valle, Diagnosis and management of adverse local tissue reactions secondary to corrosion at the head-neck junction in patients with metal on polyethylene bearings, J. Arthroplast. 31 (1) (2016) 264–268.
[6] D. Dimitriou, M.H.L. Liow, T.Y. Tsai, W.A. Leone, G.A. Li, Y.M. Kwon, Early outcomes of revision surgery for taper corrosion of dual taper total hip arthroplasty in 187 patients, J. Arthroplast. 31 (7) (2016) 1549–1554.
[7] Y.M. Kwon, S. Khormaee, M.H. Lincoln, T.Y. Tsai, A.A. Freiberg, H.E. Rubash, Asymptomatic pseudotumors in patients with taper corrosion of a dual-taper modular femoral stem MARS-MRI and metal ion study, J. Bone Joint Surg.-Am. 98 (20) (2016).
[8] J.M. Jennings, D.A. Dennis, C.C. Yang, Corrosion of the head-neck junction after total hip arthroplasty, J. Am. Acad. Orthop. Sur. 24 (6) (2016) 349–356.
[9] S.J. Incavo, Goals and challenges of identifying asymptomatic pseudotumors in patients treated with total hip arthroplasty, J. Bone Joint Surg.-Am. 98 (20) (2016).
[10] S.A. Sutphen, L.H. MacLaughlin, A.A. Madsen, J.H. Russell, M.A. McShane, Prevalence of pseudotumor in patients after metal-on-metal hip arthroplasty evaluated with metal ion analysis and MARS-MRI, J. Arthroplast. 31 (1) (2016) 260–263.
[11] Y.M. Kwon, S.J. Ostlere, P. McLardy-Smith, N.A. Athanasou, H.S. Gill, D.W. Murray, "Asymptomatic" pseudotumors after metal-on-metal hip resurfacing arthroplasty: prevalence and metal ion study, J. Arthroplast. 26 (4) (2011) 511–518.
[12] B. Behl, I. Papageorgiou, C. Brown, R. Hall, J.L. Tipper, J. Fisher, E. Ingham, Biological effects of cobalt-chromium nanoparticles and ions on dural fibroblasts and dural epithelial cells, Biomaterials 34 (14) (2013) 3547–3558.
[13] C. Nich, Y. Takakubo, J. Pajarinen, M. Ainola, A. Salem, T. Sillat, A.J. Rao, M. Raska, Y. Tamaki, M. Takagi, Y.T. Konttinen, S.B. Goodman, J. Gallo, Macrophages-Key cells in the response to wear debris from joint replacements, J. Biomed. Mater. Res. A 101 (10) (2013) 3033–3045.
[14] C.N. Serhan, J. Savill, Resolution of inflammation: the beginning programs the end, Nat. Immunol. 6 (12) (2005) 1191–1197.
[15] Z. Xia, B.F. Ricciardi, Z. Liu, C. von Ruhland, M. Ward, A. Lord, L. Hughes, S.R. Goldring, E. Purdue, D. Murray, G. Perino, Nano-analyses of wear particles from metal-on-metal and non-metal-on-metal dual modular neck hip arthroplasty, Nanomedicine 13 (3) (2017) 1205–1217.
[16] S.J. Baskey, E.A. Lehoux, I. Catelas, Effects of cobalt and chromium ions on lymphocyte migration, J. Orthop. Res. 35 (4) (2017) 916–924.
[17] J. Weischenfeldt B. Porse Bone marrow-derived macrophages (BMM): isolation and applications CSH Protoc. 2008 pdb prot5080.
[18] K.H. Martin, K.E. Hayes, E.L. Walk, A.G. Ammer, S.M. Markwell, S.A. Weed, Quantitative measurement of invadopodia-mediated extracellular matrix proteolysis in single and multicellular contexts, J. Vis. Exp. (66) (2012) e4119.
[19] Y.M. Park, M. Febbraio, R.L. Silverstein, CD36 modulates migration of mouse and human macrophages in response to oxidized LDL and may contribute to macrophage trapping in the arterial intima, J. Clin. Invest. 119 (1) (2009) 136–145.
[20] R. Mayor, S. Etienne-Manneville, The front and rear of collective cell migration Nature reviews, Mol. cell Biol. 17 (2) (2016) 97–109.
[21] C.Y. Tay, P.Q. Cai, M.I. Setyawati, W.R. Fang, L.P. Tan, C.H.L. Hong, X.D. Chen, D. T. Leong, Nanoparticles strengthen intracellular tension and retard cellular migration, Nano Lett. 14 (1) (2014) 83–88.
[22] A. Akhmanova, M.O. Steinmetz, Control of microtubule organization and dynamics: two ends in the limelight Nature reviews, Mol. Cell Biol. 16 (12) (2015) 711–726.
[23] C. Hubbert, A. Guardiola, R. Shao, Y. Kawaguchi, A. Ito, A. Nixon, M. Yoshida, X. F. Wang, T.P. Yao, HDAC6 is a microtubule-associated deacetylase, Nature 417 (6887) (2002) 455–458.
[24] I.C. Osma-Garcia, C. Punzon, M. Fresno, M.D. Diaz-Munoz, Dose-dependent effects of prostaglandin E2 in macrophage adhesion and migration, Eur. J. Immunol. 46 (3) (2016) 677–688.
[25] J.G. Evans, P. Matsudaira, Structure and dynamics of macrophage podosomes, Eur. J. Cell Biol. 85 (3–4) (2006) 145–149.
[26] K. Jomova, M. Valko, Advances in metal-induced oxidative stress and human disease, Toxicology 283 (2–3) (2011) 65–87.
[27] S. Linder, M. Aepfelbacher, Podosomes: adhesion hot-spots of invasive cells, Trends Cell Biol. 13 (7) (2003) 376–385.
[28] H.S. Gill, G. Grammatopoulos, S. Adshead, E. Tsialogiannis, E. Tsiridis, Molecular and immune toxicity of CoCr nanoparticles in MoM hip arthroplasty, Trends Mol. Med. 18 (3) (2012) 145–155.
[29] A.M. Kaufman, C.I. Alabre, H.E. Rubash, A.S. Shanbhag, Human macrophage response to UHMWPE TiAlV, CoCr, and alumina particles: analysis of multiple cytokines using protein arrays, J. Biomed. Mater. Res. A 84 (2) (2008) 464–474.
[30] R. VanOs, L.L. Lildhar, E.A. Lehoux, P.E. Beaule, I. Catelas, In vitro macrophage response to nanometer-size chromium oxide particles, J. Biomed. Mater. Res. B Appl. Biomater. 102 (1) (2014) 149–159.
[31] O.M. Posada, R.J. Tate, R.M.D. Meek, M.H. Grant, In Vitro Analyses of the Toxicity Immunological, and Gene Expression Effects of Cobalt-Chromium Alloy Wear Debris and Co Ions Derived from Metal-on-Metal Hip Implants, Lubricants 3 (3) (2015) 539–568.
[32] O.M. Posada, R.J. Tate, M.H. Grant, Effects of CoCr metal wear debris generated from metal-on-metal hip implants and Co ions on human monocyte-like U937 cells, Toxicol. In Vitro 29 (2) (2015) 271–280.
[33] P.A. Potnis, D.K. Dutta, S.C. Wood, Toll-like receptor 4 signaling pathway mediates proinflammatory immune response to cobalt-alloy particles, Cell Immunol. 282 (1) (2013) 53–65.
[34] M.C. Parry, G. Bhabra, A. Sood, F. Machado, L. Cartwright, M. Saunders, E. Ingham, R. Newson, A.W. Blom, C.P. Case, Thresholds for indirect DNA damage across cellular barriers for orthopaedic biomaterials, Biomaterials 31 (16) (2010) 4477–4483.
[35] S.B. Goodman, Wear particles, periprosthetic osteolysis and the immune system, Biomaterials 28 (34) (2007) 5044–5048.
[36] G. Perino, B.F. Ricciardi, S.A. Jerabek, G. Martignoni, G. Wilner, D. Maass, S.R. Goldring, P.E. Purdue, Implant based differences in adverse local tissue reaction in failed total hip arthroplasties: a morphological and immunohistochemical study, BMC Clin. Pathol. 14 (2014) 39.
[37] C. Le Clainche, M.F. Carlier, Regulation of actin assembly associated with protrusion and adhesion in cell migration, Physiol. Rev. 88 (2) (2008) 489–513.
[38] A.J. Ridley, M.A. Schwartz, K. Burridge, R.A. Firtel, M.H. Ginsberg, G. Borisy, J.T. Parsons, A.R. Horwitz, Cell migration: integrating signals from front to back, Science 302 (5651) (2003) 1704–1709.
[39] J.L. McGrath, Cell spreading: the power to simplify, Curr. Biol. 17 (10) (2007) R357–R358.
[40] D.A. Murphy, S.A. Courtneidge, The 'ins' and 'outs' of podosomes and invadopodia: characteristics, formation and function, Nature reviews, Mol. Cell Biol. 12 (7) (2011) 413–426.
[41] D. Ilic, Y. Furuta, S. Kanazawa, N. Takeda, K. Sobue, N. Nakatsuji, S. Nomura, J. Fujimoto, M. Okada, T. Yamamoto, Reduced cell motility and enhanced focal adhesion contact formation in cells from FAK-deficient mice, Nature 377 (6549) (1995) 539–544.
[42] N.S. Chandel, E. Maltepe, E. Goldwasser, C.E. Mathieu, M.C. Simon, P.T. Schumacker, Mitochondrial reactive oxygen species trigger hypoxia-induced transcription, Proc. Natl. Acad. Sci. U.S.A. 95 (20) (1998) 11715–11720.
[43] T. Kamiya, H. Hara, H. Yamada, H. Imai, N. Inagaki, T. Adachi, Cobalt chloride decreases EC-SOD expression through intracellular ROS generation and p38-MAPK pathways in COS7 cells, Free Rad. Res. 42 (11–12) (2008) 949–956.

[44] H. Sauer, M. Wartenberg, J. Hescheler, Reactive oxygen species as intracellular messengers during cell growth and differentiation, Cell Physiol. Biochem. 11 (4) (2001) 173–186.
[45] C.L. Bigarella, R. Liang, S. Ghaffari, Stem cells and the impact of ROS signaling, Development 141 (22) (2014) 4206–4218.
[46] M. Mittal, M.R. Siddiqui, K. Tran, S.P. Reddy, A.B. Malik, Reactive oxygen species in inflammation and tissue injury, Antioxid. Redox Sign 20 (7) (2014) 1126–1167.
[47] T.C. Meng, T. Fukada, N.K. Tonks, Reversible oxidation and inactivation of protein tyrosine phosphatases in vivo, Mol. Cell 9 (2) (2002) 387–399.
[48] G.E. Jones, W.E. Allen, A.J. Ridley, The Rho GTPases in macrophage motility and chemotaxis, Cell Adhes. Commun. 6 (2–3) (1998) 237–245.
[49] V. Konigs, R. Jennings, T. Vogl, M. Horsthemke, A.C. Bachg, Y. Xu, K. Grobe, C. Brakebusch, A. Schwab, M. Bahler, U.G. Knaus, P.J. Hanley, Mouse macrophages completely lacking Rho subfamily GTPases (RhoA, RhoB, and RhoC) have severe lamellipodial retraction defects, but robust chemotactic navigation and altered motility, J. Biol. Chem. 289 (44) (2014) 30772–30784.
[50] A.J. Ridley, Rho GTPase signalling in cell migration, Curr. Opin. Cell Biol. 36 (2015) 103–112.
[51] S. Linder, D. Nelson, M. Weiss, M. Aepfelbacher, Wiskott-Aldrich syndrome protein regulates podosomes in primary human macrophages, Proc. Natl. Acad. Sci. U.S.A. 96 (17) (1999) 9648–9653.
[52] A.R. Dwyer, K.A. Mouchemore, J.H. Steer, A.J. Sunderland, N.G. Sampaio, E.L. Greenland, D.A. Joyce, F.J. Pixley, Src family kinase expression and subcellular localization in macrophages: implications for their role in CSF-1-induced macrophage migration, J. Leukoc. Biol. 100 (1) (2016) 163–175.
[53] G.E. Jones, Cellular signaling in macrophage migration and chemotaxis, J. Leukoc. Biol. 68 (5) (2000) 593–602.
[54] S. Hanna, M. El-Sibai, Signaling networks of Rho GTPases in cell motility, Cell Signal. 25 (10) (2013) 1955–1961.
[55] S. Tojkander, G. Gateva, P. Lappalainen, Actin stress fibers–assembly, dynamics and biological roles, J. Cell. Sci. 125 (Pt 8) (2012) 1855–1864.
[56] R.L. Berdeaux, B. Diaz, L. Kim, G.S. Martin, Active Rho is localized to podosomes induced by oncogenic Src and is required for their assembly and function, J. Cell Biol. 166 (3) (2004) 317–323.
[57] M. Schramp, O. Ying, T.Y. Kim, G.S. Martin, ERK5 promotes Src-induced podosome formation by limiting Rho activation, J. Cell Biol. 181 (7) (2008) 1195–1210.
[58] N.B.M. Rafiq, Z.Z. Lieu, T.T. Jiang, C.H. Yu, P. Matsudaira, G.E. Jones, A.D. Bershadsky, Podosome assembly is controlled by the GTPase ARF1 and its nucleotide exchange factor ARNO, J. Cell Biol. 216 (1) (2017) 181–197.
[59] P. Downarowicz, M. Mikulewicz, Trace metal ions release from fixed orthodontic appliances and DNA damage in oral mucosa cells by in vivo studies: a literature review, Adv. Clin. Exp. Med.: Off. Organ Wroclaw Med. Univ. 26 (7) (2017) 1155–1162.
[60] E. Ingham, T.R. Green, M.H. Stone, R. Kowalski, N. Watkins, J. Fisher, Production of TNF-alpha and bone resorbing activity by macrophages in response to different types of bone cement particles, Biomaterials 21 (10) (2000) 1005–1013.
[61] T. Matsusaki, K. Kawanabe, K. Ise, T. Nakayama, J. Toguchida, T. Nakamura, Gene expression profile of macrophage-like U937 cells in response to polyethylene particles: a novel cell-particle culture system, J. Arthroplast. 22 (7) (2007) 960–965.
[62] E. Yagil-Kelmer, P. Kazmier, M.N. Rahaman, B.S. Bal, R.K. Tessman, D.M. Estes, Comparison of the response of primary human blood monocytes and the U937 human monocytic cell line to two different sizes of alumina ceramic particles, J. Orthop. Res. 22 (4) (2004) 832–838.